
Article:
Pratama, Y, Simone, E orcid.org/0000-0003-4000-2222 and Rappolt, M orcid.org/0000-0001-9942-3035 (2021) The Unique Crystallization Behavior of Buffalo Milk Fat. Crystal Growth & Design, 21 (4). pp. 2113-2127. ISSN 1528-7483

https://doi.org/10.1021/acs.cgd.0c01543

The Unique Crystallisation Behaviour of Buffalo Milk Fat

Yoga Pratama[1,2], Elena Simone[1] and Michael Rappolt*[1]

[1]School of Food Science and Nutrition, Food Colloids and Bioprocessing Group, University of Leeds, Leeds LS2 9JT, U.K.

[2]Department of Food Technology, Faculty of Animal and Agricultural Sciences, Diponegoro University, Jl. Prof. Soedarto Tembalang Semarang 50275, Indonesia

Abstract

Full comprehension of milk fat crystallisation is important for the structural development of dairy products such as butter, ice cream and cheese. The influence of triacylglycerols (TAGs) composition on the dynamic of milk fat crystallisation and the nanostructure of the formed crystals was investigated using two chemically different types of milk fat, namely buffalo and cow milk fat (BMF; CMF). TAG composition was determined using liquid chromatography and mass spectrophotometry (LCMS) whereas differential scanning calorimetry (DSC), small and wide-angle X-ray scattering (SAXS and WAXS) and polarised light microscopy (PLM) were used to characterise the crystallisation behaviour of the two milk fats. 37 TAG species were identified in both, BMF and CMF, but in different proportions. In particular, BMF was found to have a higher amount of low molecular weight TAGs compared to CMF. This difference in chemical composition explains the different kinetics of polymorphic transformation in the two samples. Specifically, it clarifies the delay in the nucleation of the β'-polymorph in BMF compared to CMF. BMF also showed higher nucleation rate due to its higher proportion of saturated TAGs and higher melting range. Finally, this work present a novel interpretation for the mechanism of formation of the β-polymorph (53 Å), which has recently become subject of a vivid debate in milk fat crystallisation studies.

Keywords: buffalo milk fat, crystallisation, polymorph and triacylglycerols

*Corresponding author: e-mail m.rappolt@leeds.ac.uk

1 Introduction

Buffalo milk (BM) is the second most produced type of milk, comprising 15% of the global milk production in 2018. Furthermore, the production of BM is increasing while cow milk (CM) has decreased its presence on the market from 83 to 81 % between 2014 and 2018.[1] BM is usually considered a premium product due to its greater whitening effect to tea and coffee [2] and due to its distinct melting properties that allow its use for the manufacturing of a type of mozzarella cheese known as *Mozzarella di Bufala* [3]. Most importantly, BM contains a higher level of milk solids when compared to CM (Table 1); therefore, generating higher yield of solid-based dairy products such as cheese during processing.

Table 1. Buffalo and cow milk solids composition.

Component	**Buffalo [4]**	**Buffalo [5]**	**Buffalo [6]**	**Cow [5]**
Total solids (g/100g)	16.3-18.4	16-17	17.74-19.03	12-13
Fat (g/100g)	6.6 – 9.6	5.3-15.0	6.77-7.82	3.3-6.4
Protein (g/100g)	2.7-5.2	2.7-4.7	4.54-4.92	3.0-4.0
Lactose (g/100g)	4.51-5.24	3.2-4.9	5.13-5.28	4.5-5.6
Ash (g/100g)	0.71-0.85	0.8-0.9	ND	0.7-0.8

ND: not defined.

Milk solids hold an important role in the structure development of dairy products. In particular, the structure, stability and overall quality of fat based products such as butter and ice cream is largely influenced by the milk fat crystallisation behaviour. In fact, the way milk fat crystallizes defines the size and shape distribution of crystals within the product and also their internal nanostructure (polymorphism). All these crystal properties dictate important quality attributes of dairy products, such as mouth-feel, melting point, spread-ability, texture, and rheological properties.[7]

Milk fat is a complex fat comprising of a wide variety of different TAGs. Identification of fat polymorphism is commonly investigated with X-ray scattering techniques. The periodicity of crystal structures give rise to X-ray diffraction patterns which can be observed in the small and wide angle regions, which correspond to the long and short spacings, respectively.[8] The long spacings correspond to the longitudinal, lamellar stacking of TAG molecules, displaying mostly two (2L) or three (3L) chain length repeating planar structures. On the molecular level, the short

spacings indicate the fat crystal sub-cell or lateral packing structure, which commonly denoted as sub-α (γ), α, β' and β polymorph, in the order of increasing stability.[9,10]

For advancing our understanding on the unique crystallisation behaviour of BMF in this study, we will discuss our findings in relation to other, mainly CMF investigations, that were focussed on the crystallisation behaviour, determining the role of TAGs and fatty acids composition,[11–13] fractionation process,[14,15] cooling rates,[10,16,17], shear rate,[18] the presence of minor components,[19] solvent addition,[20] and other processing conditions.[21] At least five crystalline sub-cell species have been observed in milk fat: α and sub-α, two β' and one β type polymorphs, several of them were found in coexistence, depending on the thermal profile applied to generate milk fat crystals. Lamellar structures with 2L-architecture were found to display thicknesses between 4 to 4.8 nm and 3L-lamellar organizations of TAG are reported to have thicknesses from 5.4 to 7.2 nm.[22] All these crystalline structures always appear to coexist with the isotropic liquid phase, even at low temperature (e.g., 4 °C).[16]

Among all sub-cell species, the α- and β'-polymorph of milk fat are the most common, while sub-α and β-polymorph are only rarely observed.[10,16,23] The polymorphism of milk fat was found to be strongly affected by TAGs and fatty acids composition. In particular, the olein-rich fraction of milk fat can crystallise only in the α-polymorph, while both α- and β'-polymorph can form in the stearin-rich fractions upon cooling at 1 °C/min.[11] The sub-α (γ) form was only reported to appear upon fast cooling below -8 °C.[10,16] On the bases of WAXS measurements, this polymorph was described as a low-melting β′-modification with orthorhombic chain packing. The presence of a β-polymorph in milk fat has been subject of debate, as this structure was not found in milk fat,[10] or forming only via applying a fast cooling rate followed by an isothermal hold for long time.[24] Further, experimental evidence suggests that the stability and kinetics of crystallisation of this crystal structures are affected by the TAGs and fatty acids composition of milk fat. Tzompa-Sosa, et al.[12] studied the crystallisation behaviour of different milk fat samples of varying TAGs composition and found that the nucleation of the β-polymorph was promoted by the presence of unsaturated TAGs with carbon numbers around 52-54. Nevertheless, the same study showed that the β'-polymorph was the dominant structure in most samples at ambient conditions.

The TAG' configurational symmetry has been linked with polymorphic outcome during crystal formation.[25] In general, TAGs containing uniform or symmetrical fatty acids follow the typical α → β'→ β transformation. Whilst, asymmetrical TAGs, i.e., TAGs with combination of UUS

or SSU, in which the solitary unsaturated (U) or saturated (S) fatty acid resides on either the sn-1 or sn-3 position or TAG with acyl chain length differences greater than 2 carbon atoms, are more prevalent in the β'-polymorph. A previous study also showed that milk fat comprise of many asymmetrical TAGs, which contain short chain butyric acid.[11]

The types of TAGs and fatty acids in milk fat depends on the season and the geographical regions where cows are grown;[13,26] and these variations, albeit small, can strongly affect crystallisation behaviour.[13,27] Compositional differences in milk fats obtained from different animals (e.g., buffalo *vs.* cow) are more significant than variation within the same species.[5,28] Those differences are currently not fully characterized, but they could have a significant impact on the crystallisation and melting behaviour of milk fat; as shown by a small number of crystallisation studies carried out on non-bovine milk fat, such as goat and camel.[29–32]

The TAGs composition of milk fat can be investigated using various chromatography techniques, combined with molecular mass identification analysis.[33–36] Previous studies[4,28,37–39] only determined the fatty acids composition and total carbon number of each TAG forming buffalo milk fat, indicating that buffalo milk fat has a higher content of saturated fatty acids (SFA) compared to cow milk fat.[2,4,28] To the best of our knowledge, the current work is the first to determine exactly the TAGs composition of buffalo milk fat, and to investigate how the individual, structural configuration of TAGs in this type of fat affect its crystallisation and melting behaviour. The aim of our study is to compare the crystallisation behaviour of buffalo and cow milk fat, particularly the dynamics of α, β', and β -polymorph formation, and understand the role played by the TAG compositional differences.

The results presented here will allow a more rational design of novel dairy products for targeted applications (e.g., products with higher crystallinity or more stable polymorphs for tropical countries' markets) as well as promote a more widespread use of buffalo milk fat.

2 Materials and Methods

2.1 Sample preparation

Milk fat (ghee) was prepared from unsalted butter following the heat clarification method.[40] Unsalted La Marchesa buffalo butter was purchased from La Marchesa (Terevola-Italy) and unsalted Lurpak cow butter (Arla Foods, Denmark) was obtained from a local grocery store. The two types of butter contain approximately 82% of milk fat. 250 g of butter was heated to a temperature of 110-120 °C for at least 15 minutes, under constant stirring in order to remove the moisture. Heating was stopped when no more water vapour bubbles were observed (indicating complete removal of water), and the molten butter turned clear with visible suspended solid (milk protein) at the bottom. The milk fat was separated by the precipitated solids by filtering the molten butter it through three layers of fine muslin cheese cloth (Homestead Farm Supplies, Banbury-UK). The resulted milk fat contained ≥ 99.5% of fat, as confirmed in a total fat analysis using the Soxhlet method. Resulted milk fat was then kept in amber bottle at chill temperature for further analysis.

2.2 Analysis of milk fat TAG composition

LCMS grade isopropanol, acetic acid and ammonium acetate (Optima LC/MS) were obtained from Fisher Chemical (USA). LCMS grade methanol (LichroSolv) was obtained from Merck (Germany). Lipid standards: a standard TAG mixture (17811-1AMP) was obtained from Sigma-Aldrich (Merck KGaA, Darmstadt, Germany). Acetone was obtained from VWR Chemicals. Nylon syringe filter 0.22µm was purchased from Gilson Scientific Ltd (Dunstable-UK).

25 mg of milk fat was added to 2 ml of acetone and 2 ml of 18% (v/v) isopropanol in methanol (IPA/MeOH). Further dilution was carried out using acetone and IPA/MeOH 1:1 (v/v) until the final concentration of 250 µg/ml. For complete dissolution, the sample was subsequently heated in a water bath at 70 °C for 5 minutes to avoid the reprecipitation of solid milk fat in the cold solvent. The mixture was then filtered using a nylon syringe filter and inserted into the injection vial. A TAG mixture standard was prepared with the same procedure.

Milk fat TAG composition measurements were performed according to the procedure described by Zeb and Murkovic[41] using a Shimadzu LCMS 2020 (Japan) and processed with the LabSolutions software (version 5.97). A separation column Phenomenex Luna 3u C18(2) 100A

LC Column 150 x 3.0 mm was used. The mobile phase consisted of 18% (v/v) isopropanol in methanol (0.1% (v/v) acetic acid) plus 0.05% (v/v) of ammonium acetate. The samples were eluted in an isocratic system with flow rate of 0.6 ml/min. The spectrometric conditions were: positive ESI mode, fragmentor potential of 150 V, drying gas temperature of 350 °C and capillary voltage of 4000 V. The column oven and autosampler chamber temperature were maintained at 40 °C in order to ensure dissolution of the fat samples. The mass spectra were obtained at an m/z range of 200 to 1000 with an elution time of 50 minutes. Each sample was measured in 4 replicates. The TAG mixture standard was used as a control of the method efficiency and as an internal standard.

The identification of chromatogram peak was achieved by mass spectra analysis where main spectra corresponds to the TAG molecular weight [41]. Whilst the fragments spectra could be used to identify the TAG configuration because fatty acid at sn-2 position tended to be easier to be lost than that at sn-1/3 positions [35,41]. However, the present study fragments spectra intensity were not strong enough to make a justifiable positional isomer identification. Hence the present TAG configuration is based on existing literature with similar spectra profiles [35] with possibility of other isomer configuration.

Perpendicular separation[42] was uniformly applied to less-resolved peaks. Relative concentration of each TAG is calculated as the ratio between a specific peak area and the total area resulting from the sum of all the recorded peaks (including the non-TAG-identified peak areas). Statistical analysis of the data was carried out using the *t-Test* routine in Microsoft Excel Analysis ToolPak, where a p-value <0.05 indicates a statistical significance. OriginPro 2018 (OriginLab, Massachusetts, USA) was used for data pre-processing, including baseline correction and peak intensity normalisation using the highest-intensity peak.

2.3 *Differential scanning calorimetry (DSC) measurements*

Samples of molten milk fat (10±3 mg) were weighed and sealed hermetically in aluminium pans (Tzero, TA Instruments, Elstree-UK). The exact weight of each sample was used to normalise the acquired heat flow data and an empty pan was used as a reference. Heat flow measurements were performed in a DSC Q-20 (TA Instruments, Elstree-UK) following a cooling and heating cycle with three different scan rates, i.e., 0.5, 2 and 10 °C/min. The samples were brought to 60 °C and held at such temperature for 10 minutes, to erase any crystal memory

before being cooled down to -40 °C with the aforementioned rates. The samples were held at -40 °C for 5 minutes, before being subjected to a heating ramp back to 60 °C using the same scan rate as before. The data analysis was performed using TA Universal Analysis 2000 software (version 4.5A). Subsequent baseline correction, plotting and integration of the peaks were carried out using the OriginPro 2018 software. All measurements were performed in four replicates and data were presented as average value ± standard deviation. *t-Test* analysis on the relative concentration of each milk fat fraction was performed in Microsoft Excel Analysis.

2.4 X-ray scattering measurements and analysis

Small angle X-ray scattering (SAXS) and wide angle X-ray scattering (WAXS) measurements were carried out with a SAXSpace instrument (Anton Paar GmbH, Graz, Austria). The instrument uses a Cu-anode (λ = 0.154 nm) and operates at 40 kV and 50 mA. The sample chamber is equipped with a TCstage 150 Peltier element (Anton Paar GmbH, Graz, Austria), which provides a temperature control in a range of -30 to 150 °C (± 0.1 °C). Simultaneous SAXS/WAXS measurements were performed at a sample-detector distance (SDD) of 130 mm, which cover a q-range from 0.01 to 1.76 Å^{-1} ($q = 4\pi \sin\theta/\lambda$ with 2θ being the scattering angle). The 1D scattering patterns were recorded with a Mythen micro-strip X-ray detector (Dectris Ltd, Baden, Switzerland).

Milk fat samples were molten on a hot plate prior to injection quartz disposable capillaries (Capillary Tube Supplies Ltd., Cornwall-UK) of outside diameter of 1.5 mm. The capillaries were subsequently sealed with wax and epoxy glue.

SAXS/WAXS measurements were carried out using three thermal protocols. First, milk fat samples were heated to 60 °C and equilibrated for 10 minutes in order to completely melt and erase any crystal memory. This was followed by cooling at 2 °C/min to -10 °C and final isothermal conditions for 5 hours. A 60 s exposure time was used to collect X-ray patterns every 30 minutes during isothermal conditions. The second thermal protocol included the melting procedure previously described followed by cooling at three different rates, i.e., 0.5, 2 and 4 °C/min down to -10 °C. A 30 s exposure time was used to collect measurements every minute during the cooling ramp. In the third protocol, the capillaries were stored in a freezer (*ca*. -18 °C) for three weeks and subsequently transferred into the SAXSpace sample chamber. The

samples were equilibrated at -10 °C for 15 minutes, followed by heating at 2 °C/min to 60 °C. X-ray patterns were collected every minute with an exposure time of 30 s.

The position of the primary beam of all diffraction patterns was set to zero using the SAXSTreat software (Anton Paar GmbH, Graz, Austria). Using the SAXSQuant software (Anton Paar GmbH, Graz, Austria), all recorded scattering patterns were normalised for their transmission, i.e., divided by their measured transmitted direct beam intensity. From each normalised sample pattern the normalised empty capillary scattering was then subtracted. The resulting patterns were smeared in the small angle regime, approximately from $q = 0$ to $q = 0.25$ Å^{-1}, due to the line collimation focus of the X-ray camera. In few cases (as indicated in the results section), the scattering contribution from molten TAG was also subtracted from the total pattern. OriginPro 2018 was used for plotting the patterns and for carrying out peak fit analysis.

Electron Density Profile (EDP) determination by classical Fourier analysis: EDPs of the α-, β'- and β-phases were determined by standard procedures.[43,44] In brief, the Bragg diffraction peaks were fitted by a Lorentzian distribution function and additionally fitting the diffuse scattering contributions with second degree polynomials. The intensities were Lorentz corrected (note, for our quasi line-focus set-up with 20 mm width by 0.2 mm height, an experimentally determined correction factor of $h^{1.5}$ was applied; this compares to a Lorentz correction for an ideal point focus of h^2 and for an ideal line focus of h, respectively), and finally, the square root of the corrected intensities resulted in the form factor values, F_h. Note, in case of centrosymmetric EDPs, the Fourier transform is obtained by the summation of cosine terms only:

$$\Delta\rho(z) = \sum_{h=1}^{h_{max}} \alpha_h F_h cos\left(\frac{2\pi z h}{d}\right) \qquad \text{(Eq. 1)}$$

where $\Delta\rho$ is the electron density contrast, h the Miller index (diffraction order), α_h the phases (note, α_h is fixed to -1 for $h = 1$ and ±1 for $h > 1$), z is the real space variable, i.e., describing the real-space axis perpendicular to the lamellae, and d denotes the lattice spacing. The phases α_h for $h > 1$ were taken from literature [45] (determined F_h and applied phases are listed in Table S2 and S3).

2.5 Polarized Light Microscopy (PLM) measurements

Milk fat crystals formed during cooling crystallisation experiments were observed using a Leitz Dialux 22 microscope (Leitz, Wetzlar, Germany) at 40x magnification, coupled with a Canon EOS 7D Mark II (Canon, Japan) digital camera. A Linkam CSS 450 hot stage (Linkam Instruments, Tadworth-UK) and the Linksys 32 software data capture system (Linkam Instruments, Tadworth-UK) were used to control the temperature profile during the crystallisation. 50 µL of milk fat sample was placed in the hot stage sample chamber with the thickness (gap) set to 100 µm. The sample was brought to 60 °C for 10 minutes in order to melt any crystal present. Subsequently, the samples were cooled at 0.5 or 2 °C/min. Images (4864 x 3648 pixel) were collected during the crystallization process and scaled using 1 mm graticule at the same resolution. The image contrast was enhanced for publication purpose and the area, A, of each crystalline object was measured individually using the freehand tool of ImageJ 1.53a software (NIH, USA). The crystal size is expressed with its diameter, D, assuming a nearly circular section of the crystals with $D = \sqrt{(4A/\pi)}$.

3 Results and Discussion

3.1 TAG composition of BMF and CMF

As shown in Figure 1 and Table 2, 38 different TAGs from BMF and CMF were separated in the present work, and 37 of them have been successfully identified. Figure S1 and Table S1 in supplementary information present details on the peak identification procedure.

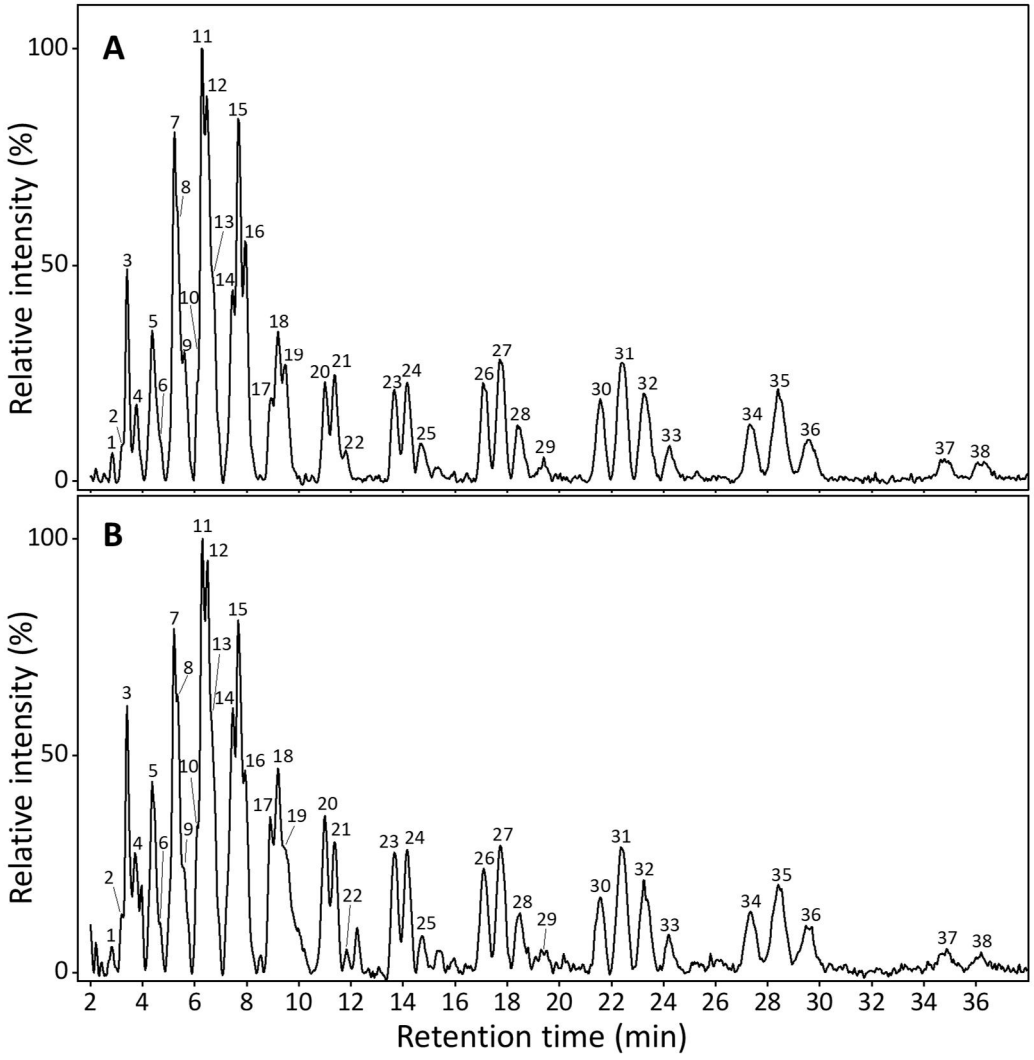

Figure 1. Baseline-corrected chromatograms of (A) buffalo milk fat and (B) cow milk fat triacylglycerol composition. For the identified triacylglycerol 1 to 38 refer to Table 1.

Table 2. Compositional characterisation of buffalo milk fat and cow milk fat.

Peak#	RT (min)	TAG Structure*	$[M+ NH_4]^+$	TAG weight fraction (% w/w) (mean ± SD) *n=4*		
				BMF	**CMF**	***p***
1	2.8	Bu-Co-P	516.4	1.10±0.18	1.23±0.22	0.400
2	3.2	Bu-C-M	544.5	1.27±0.39	0.77±0.10	0.087
3	3.4	n/i	750.5	2.98±0.26	2.70±0.19	0.147
4	3.8	Bu-C-P	572.5	2.08±0.26	1.72±0.22	0.084
5	**4.4**	**Bu-La-P**	**600.5**	**2.61±0.15**	**2.32±0.15**	**0.038**
6	4.5	Bu-La-O	626.5	2.14±0.34	2.01±0.11	0.491
7	5.2	Bu-M-P	628.5	4.28±0.31	4.16±0.17	0.514
8	**5.3**	**Bu-M-O**	**654.5**	**3.12±0.44**	**2.42±0.21**	**0.045**
9	**5.6**	**Bu-P-L**	**680.5**	**2.91±0.27**	**2.44±0.20**	**0.031**
10	6.1	Co-M-P	656.6	1.65±0.22	2.03±0.25	0.059
11	**6.3**	**Bu-P-P**	**656.6**	**5.32±0.24**	**4.27±0.22**	**0.001**
12	**6.5**	**Bu-P-O**	**682.6**	**4.49±0.35**	**3.54±0.28**	**0.005**
13	**6.7**	**Bu-O-O**	**708.6**	**3.69±0.18**	**3.18±0.29**	**0.031**
14	**7.5**	**Co-P-P**	**684.6**	**3.11±0.08**	**3.74±0.22**	**0.006**
15	**7.7**	**Bu-P-S**	**684.6**	**4.57±0.36**	**3.93±0.24**	**0.032**
16	**7.9**	**Bu-S-O**	**710.6**	**3.48±0.17**	**2.62±0.19**	**0.001**
17	**8.9**	**P-P-Cy**	**712.6**	**1.33±0.14**	**1.92±0.02**	**0.003**
18	9.2	Co-S-P	712.6	2.44±0.14	2.75±0.21	0.055
19	9.5	P-Cy-O	738.7	2.28±0.28	2.63±1.01	0.550
20	**11.0**	**P-P-C**	**740.7**	**1.74±0.05**	**2.62±0.18**	**0.002**
21	**11.4**	**P-C-O**	**766.7**	**1.90±0.06**	**2.40±0.07**	**<0.001**
22	**11.8**	**C-O-O**	**792.7**	**0.82±0.09**	**1.14±0.08**	**0.002**
23	**13.7**	**La-P-P**	**768.7**	**1.72±0.09**	**2.09±0.08**	**0.001**
24	**14.2**	**P-La-O**	**794.7**	**2.01±0.08**	**2.38±0.08**	**0.001**
25	**14.7**	**P-M-L**	**820.7**	**1.36±0.06**	**1.62±0.09**	**0.005**
26	17.1	M-P-P	796.7	2.08±0.12	2.11±0.09	0.732
27	17.7	P-M-O	822.7	2.95±0.18	2.91±0.04	0.682
28	18.4	O-M-O	848.7	2.39±0.02	2.43±0.11	0.550
29	19.4	O-P-L	874.7	1.80±0.12	1.78±0.14	0.858
30	**21.6**	**P-P-P**	**824.7**	**2.09±0.12**	**1.86±0.11**	**0.034**
31	22.4	O-P-P	850.7	3.65±0.20	3.35±0.12	0.055
32	23.2	P-O-O	876.8	3.42±0.24	3.31±0.14	0.467
33	24.2	O-O-O	902.7	1.72±0.12	1.71±0.13	0.925
34	**27.3**	**P-P-S**	**852.8**	**1.67±0.08**	**1.39±0.12**	**0.015**
35	**28.4**	**S-P-O**	**878.8**	**2.66±0.15**	**2.27±0.07**	**0.010**
36	29.6	O-O-S	904.8	1.50±0.04	1.43±0.17	0.442
37	34.8	S-P-S	880.8	0.72±0.07	0.64±0.10	0.242
38	**36.3**	**S-S-O**	**906.8**	**0.66±0.06**	**0.56±0.02**	**0.036**
Non-identified molecules				**8.30**	**11.59**	
Total				**100**	**100**	

RT: retention-time; TAG: triacylglicerols; $[M+NH_4]^+$: molecular mass of TAG + ammonium ion; BMF: buffalo milk fat; CMF: cow milk fat; *n*: number of measurements; SD: standard deviation; *p*: value of ≤ 0.5 indicate statistical significance; Bu: butyric (C4), Co: caproic (C6), Cy: caprylic (C8), C: capric (C10), La: lauric (C12), M: myristic (C14), P: palmitic (C16), S: stearic (C18), O: oleic (C18:1), L: linoleic (C18:2) fatty acid. Results in bold show significant difference between BMF and CMF weight fraction ($p<0.05$). *TAG configuration includes possible positional isomers, e.g., OOS and OSO.

Figure 1 shows that BMF and CMF present similar TAG species. Out of 37 identified TAG, 13 were asymmetrical (fatty acids with acyl chain length difference greater than two carbon atoms[25]), where the low carbon number butyric acid is attached to longer chained fatty acids like palmitic or oleic acid. 17 of the TAGs identified were fully saturated, 13 contained one unsaturated fatty acid and 7 were contained more than one. The weight fractions of each CMF TAG in this work are in agreement with a previous study, where BuPP, BuMP, BuPO, OPP, and POO were among the most abundant TAGs.[11] The most abundant TAGs in BMF are BuPP, BuPS, BuPO and BuMP.

Notwithstanding the similarity in TAG species, BMF has 20 out of 37 TAGs whose weight fractions are significantly different from CMF. This includes BuMO, BuPP, BuPO, BuOO, CoPP, BuPS, and BuSO, which were found to be present in BMF in weight fraction >3%. BMF is known to have a higher amount of saturated fatty acids compared to CMF.[4] This was confirmed by the results present here, which show that fully saturated TAGs such as PPP and PPS are more abundant in BMF compared to CMF (significantly different ratios, $p<0.05$). PPP and PPS weight fractions are 2.09% and 1.67% in BMF versus 1.86% and 1.39% in CMF. Another fully saturated TAG, SPS was also found in higher concentration in BMF compared CMF, albeit the difference was statistically insignificant (Table 2).

A complete comparison of BMF and CMF in terms of weight fractions of TAG is shown in Figure 2. BMF had a higher number of TAG exiting the chromatographic column at early and late retention-time compared to CMF. In contrast, CMF had more TAG exiting at medium retention-times.

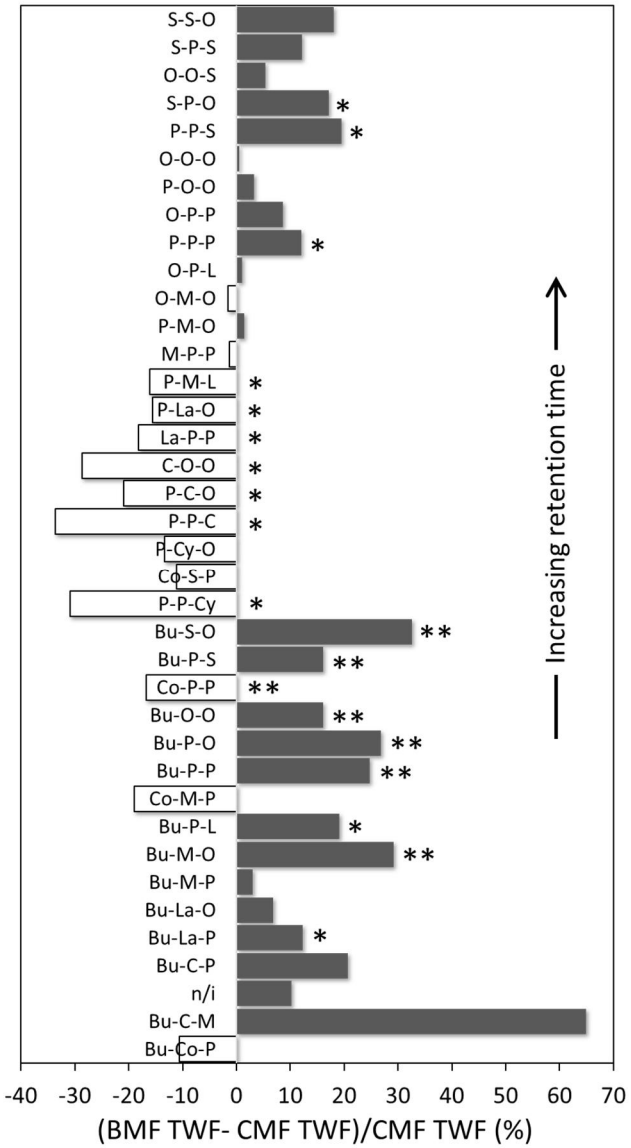

Figure 2. Percentage difference of buffalo milk fat (BMF) compared to cow milk fat (CMF) triacylglycerol (TAG) composition. Positive values indicate higher relative TAG concentration in BMF. TWF: triacylglycerol weight fraction, for other abbreviations refer to Table 1. TAG configuration includes possible positional isomers, e.g. OOS and OSO. *The difference between both fats is statistically significant (p<0.05).**The difference between both fats is statistically significant (p<0.05) and the TAG weight fraction is >3% in one or both milk fats.

Early retention-time TAGs containing capronic acid (BuCoP, CoMP and CoPP) were found in lower concentrations in BMF compared to CMF. Whereas BMF contained more TAGs presenting butyric acid. The latter finding is in agreement with previous literature.[28] In addition to the identified TAGs, the amount of unknown matters (including the non-identified peak number 3) were 11.28% and 14.29 % for BMF and CMF, respectively. This portion most likely

comprises DAGs and other TAGs in smaller amount, which could not be identified with the current separation and identification procedures.[11,35]

3.2 Thermal characterization of BMF and CMF

DSC cooling and heating thermograms for CMF and BMF are shown in Figure 3. The thermograms of the cooling step (Figure 3 A, B, C) show that both BMF and CMF exhibited two exothermic peaks, which corresponded to the crystallisation of α-2L and α-3L polymorphs, respectively.[22] It was found that onset nucleation temperatures were higher, when the cooling rate decreased (as summarized in Table 3). For instance, at 10 °C/min cooling rate, the α-2L nucleated at 17.4 °C and 15.6 °C for BMF and CMF, respectively. Whereas, at 0.5 °C/min cooling rate, the nucleation started at 19.1 °C and 17.9 °C. These results are readily understood, since slower cooling rates offer more time for nuclei of critical size to form, thus nucleation processes are expected to be observed at lower degrees of undercooling compared to faster cooling rates.

It is interesting to note, that the onset nucleation of BMF occurred at a higher temperature than that of CMF at all three cooling rates (Table 3). In descending order of cooling rates (10, 2 and 0.5 °C/min), the BMF α-2L nucleated at 17.4, 18.7, and 19.9 °C, whilst the CMF α-2L nucleated at 15.6 °C, 16.6 and 17.9, respectively. Similarly, the onset nucleation of BMF α-3L also occurred at higher temperature than CMF. BMF α-3L nucleation was observed at 13.4, 14.9 and 13.7 °C (versus 10.4, 11.7 and 11.9 °C in CMF) for 10, 2 and 0.5 °C/min cooling rate. These findings are consistent with the chromatographic measurements. The higher nucleation temperature in BMF is attributed to higher content of fully saturated TAGs. These molecules, especially the long-chained PPP, PPS and SPS have the highest melting point among all other TAGs present in milk fat.

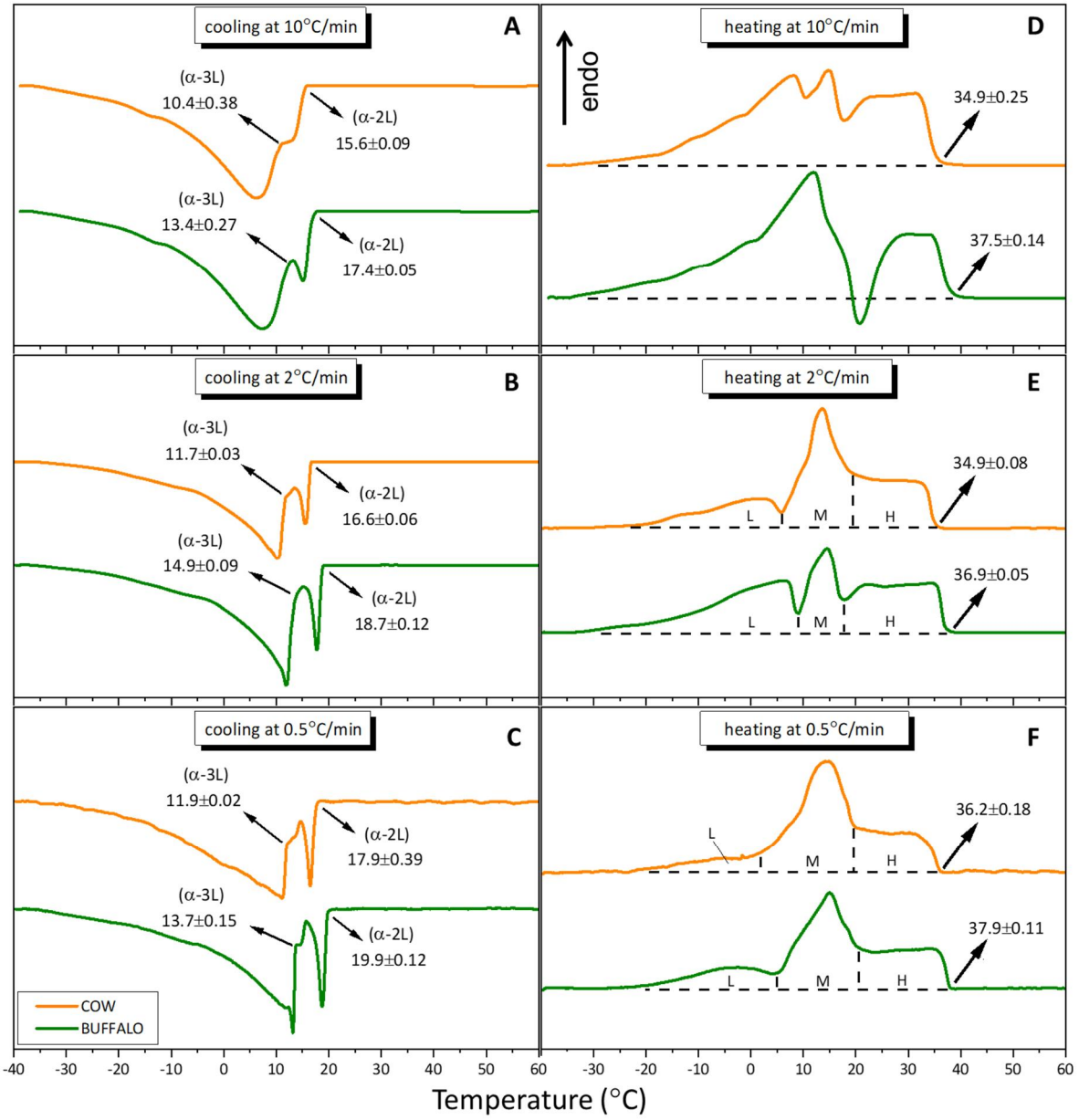

Figure 3. Thermograms of buffalo milk fat and cow milk fat on cooling (A, B, C) and on subsequent heating scans (D, E, F). Both, cooling and heating scans were carried out in the temperature interval of 60 °C to -40 °C. The applied scan-rates were 10, 2 and 0.5 °C/min, respectively. Arrows indicate associating crystallization and melting events. L, M, and H indicate three distinguished melting fractions, see Table 4.

Figure 3 (D, E, F) show the BMF and CMF thermograms of the subsequent heating step after cooling. CMF typically displays three overlapping endothermic peaks, possibly as a result of three groups of TAGs that melt consecutively, namely the low-melting, middle-melting and high-melting fractions.[10,46] A previous study suggests that the presence of this peaks is a combined effect of the melting of each fractions and polymorphic transformations. Lopez et

al.[47] reported the structural evolution of sub-α ↔ α → β' → liquid on the heating of milk fat globules at 2 °C/min after cooling at 1 °C/min. The current work is in agreement with the previous studies, where CMF exhibited three endothermic clustered peak-regions at all three different heating rates (10, 2 and 0.5 °C/min). In contrast, BMF showed three endothermic peak-regions only for the 2 and 0.5 °C/min heating rate. At 10 °C/min, we observed two endothermic and one exothermic peak. The position and shape of the endothermic peaks depends on the cooling rate, as different rates can result in different crystal polymorphs being formed.[14,22] It is also plausible that the exothermic peak represents a polymorphic transformation, as such transformations during the melting process are influenced by the heating rate.[47] Nonetheless, the current result indicates that BMF forms distinctly different polymorphs, when applying a 10 °C/min cooling and heating rate.

Table 3. *Onset of* nucleation and *end of* melting temperature of buffalo milk fat and cow milk fat at different rates.

Event		Rate (°C/min)		
		0.5	**2**	**10**
Onset of α-2L (°C)	**BMF**	19.9±0.12	18.7±0.12	17.4±0.05
	CMF	17.9±0.39	16.6±0.06	15.6±0.09
	***p*-value**	0.006	0.002	0.004
Onset of α-3L (°C)	**BMF**	13.7±0.15	14.9±0.09	13.4±0.27
	CMF	11.9±0.02	11.7±0.03	10.4±0.38
	***p*-value**	0.002	<0.001	0.005
End of Melting (°C)	**BMF**	37.9±0.11	36.9±0.05	37.5±0.14
	CMF	36.2±0.18	34.9±0.08	34.9±0.25
	***p*-value**	0.04	0.005	0.06

BMF: buffalo milk fat; CMF: cow milk fat; values presented as mean ± SD, $n = 4$.

BMF shows an about 2 °C higher melting point compared to CMF (Table 3). The BMF melted completely at 37.5, 36.9, and 37.9 °C (versus 34.9, 34.9, and 36.2 °C in CMF) for 10, 2, and 0.5 °C/min heating rate, respectively. This result is explained by the fact that BMF has a significantly higher amount of fully saturated TAGs compared to CMF. Another aspect influencing the thermal stability concerns the polymorphic form, where more stable polymorphs (such as β' and β) have higher melting points than the metastable α polymorphs. In this respect, the 0.5 °C/min scan rate displayed the highest melting points for both milk fats, because the preceding slower cooling ramps lead to the formation of more stable polymorphs. ~~whereas higher cooling rates tend to produce mainly metastable polymorphs.~~

We further measured the area under the endothermic peaks recorded at 2 and 0.5 °C/min heating rate for both, BMF and CMF. These values are largely related to the enthalpy of fusion of each melting fraction in the milk fat, and therefore, to their relative concentrations (Table 4). There are significant differences between the estimated BMF and CMF relative melting fractions. At both heating rates, BMF was found to be higher in the low- and high-melting fractions, whilst CMF was found higher in the middle-melting fraction. As mentioned previously, the endothermic profile is largely influenced by the cooling/heating rate, thus the difference in estimated melting/enthalpy fraction contribution at 2 and 0.5 °C/min heating rate was expected. A more distinct difference was found at 2 °C/min heating rate, where BMF low-, middle- and high- melting enthalpy fractions were 41.1, 22.2, and 36.7 % compared to 22.8, 48.7 and 28.5 % in CMF, respectively.

Table 4. Milk fat fractions' relative concentration of buffalo milk fat and cow milk fat.

Heating rate (°C/min)	MP fraction	Enthalpy Fraction (%) mean±SD, *n=4*		
		BMF	**CMF**	***p***
2	**low**	41.1 ±0.4	22.8 ± 0.6	<0.001
	middle	22.2 ± 0.2	48.7 ± 1.7	<0.001
	high	36.7 ± 0.5	28.5 ± 1.5	<0.001
0.5	**low**	18.8 ± 0.4	13.3 ± 1.2	0.001
	middle	50.0 ± 0.8	58.7 ± 1.3	<0.001
	high	31.2 ± 1.1	28.0 ± 0.3	0.011

MP: melting point, BMF: buffalo milk fat; CMF: cow milk fat.

Nevertheless, the BMF and CMF enthalpy fractions comparison was consistent for both heating rates, with BMF displaying greater low- and higher-melting fractions. The most plausible explanation for this trend lies their difference in TAG composition. As shown in Figure 2, the chromatographic data are consistent with the DSC thermal analysis.

3.3 Nanostructural analysis of the two α- and two β'-polymorphs in BMF and CMF

The nanostructural polymorphs of BMF and CMF upon crystallisation were evaluated. After a quenching step from 60 °C with cooling rate of 2 °C/min, the evolution of the small- and wide-angle X-ray scattering patterns of both milk fats were observed, while holding the samples isothermally at -10 °C for 5 hours (Figure 4).

At the beginning of the isothermal hold (t = 0 hour), both BMF and CMF exhibited a crystal structure with hexagonal chain packing (α-polymorph), as shown by the presence of a single short spacing of 4.15 Å. Concomitantly, as apparent from the SAXS patterns, two crystal lattices with distinct stacking organisations with d-spacing of 48.4 Å (α-2L) and 72.8 Å (α-3L) were observed. The α-3L displayed stronger scattering intensity than the α-2L polymorph. Lopez et al.[11] reported similar finding, where the α-polymorph was observed, when CMF was cooled with 1 °C/min rate, displaying three different crystalline phases, i.e., the α-2L (47 Å), α-2L (42 Å) and α-3L (72 Å) polymorph. Note, the α-2L (42 Å) was not identified in our study. Finally, the α-2L and α-3L polymorphs start to transform after 1.5 hours into their corresponding β'-2L and β'-3L polymorphs (Figure 4), which we will discuss in further detail later on.

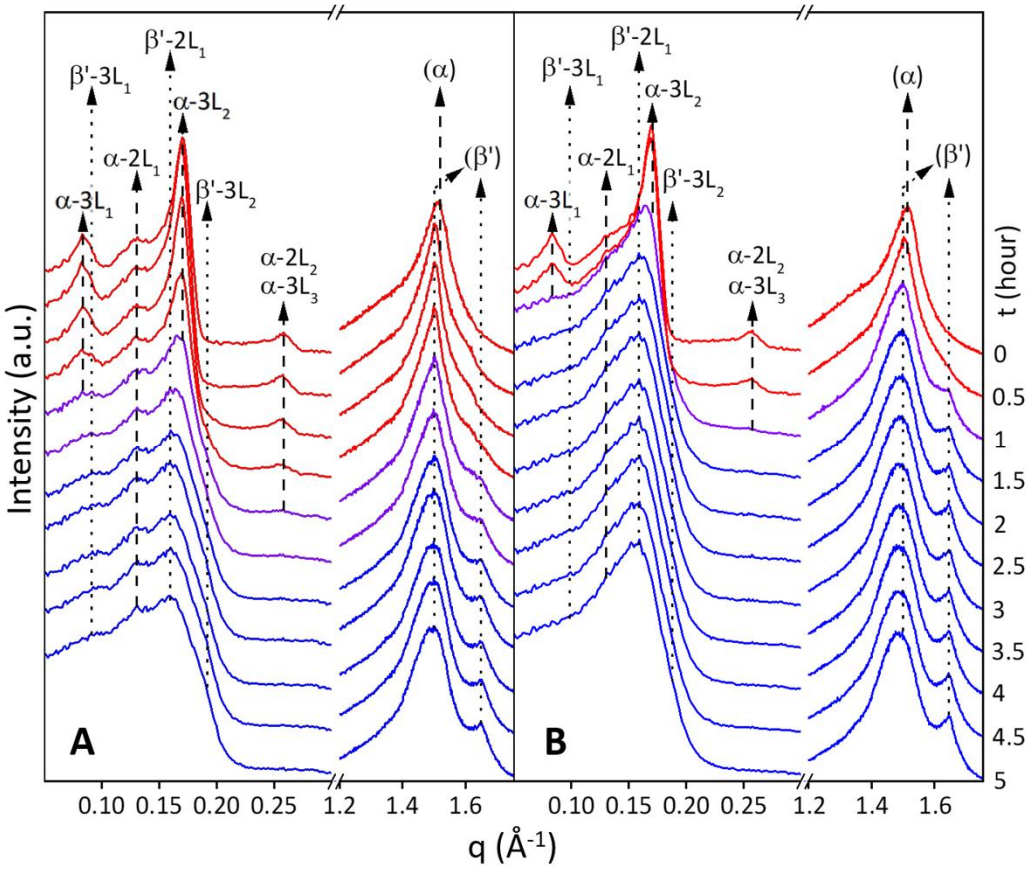

Figure 4. X-ray diffraction patterns of (A) buffalo milk fat and (B) cow milk fat in isothermal condition at -10 °C for 5 hours after cooling from 60 °C at -2 °C/min. Red lines/dashed arrows: α-polymorph, blue lines/dotted arrows: β'-polymorph, purple lines: polymorphic transition.

The similar *d*-spacing of BMF and CMF can be attributed to the similarity in TAG species, albeit differences in their relative concentrations. The *d*-spacing in TAG crystals, either in 2L or 3L stacking configuration, is dictated by the carbon chain length of the contributing TAGs and the possible tilt angles of the hydrocarbon chain with respect to the stacking direction. The α-2L phase is commonly accepted to have a hydrocarbon chain tilt angle of 0° due to their free chain rotational mode, as reflected in the hexagonal chain packing and as confirmed for pure TAG samples with known hydrocarbon chain length.[45] Therefore, since BMF has a similar *d*-spacing in the α-2L-phase as CMF we can conclude that their average chain-length compositions is alike in this polymorphic phase. Further, it is possible to estimate the average number of carbons, N_C, per hydrocarbon chain in the α-2L-phase. Since the average C-C bond length projected on the hydrocarbon chain of is known to be 1.27 Å[48] and the glycerol backbone extension in stacking direction is about 8 Å[44], we obtain:

$$d = 2\,(N_C\ 1.27\text{Å}) + 8\text{Å} \text{ or } N_C = (d - 8\text{Å})/2.54\ \text{Å} \qquad \text{(Eq. 2)}$$

Figure 5 shows the electron density profiles (EDPs) of BMF of the α-2L, α-3L, β'-2L and β'-3L polymorphs as observed at -10 °C. For all 3L-polymorphs, the overall *d*-spacing can be further decomposed into a saturated-rich bilayer chain region, d_S, and into an unsaturated-rich chain region, d_U, in which the chains pack in an interdigitated fashion. Hence, in the 3L-phase the overall lattice spacing $d = d_S + d_U$.

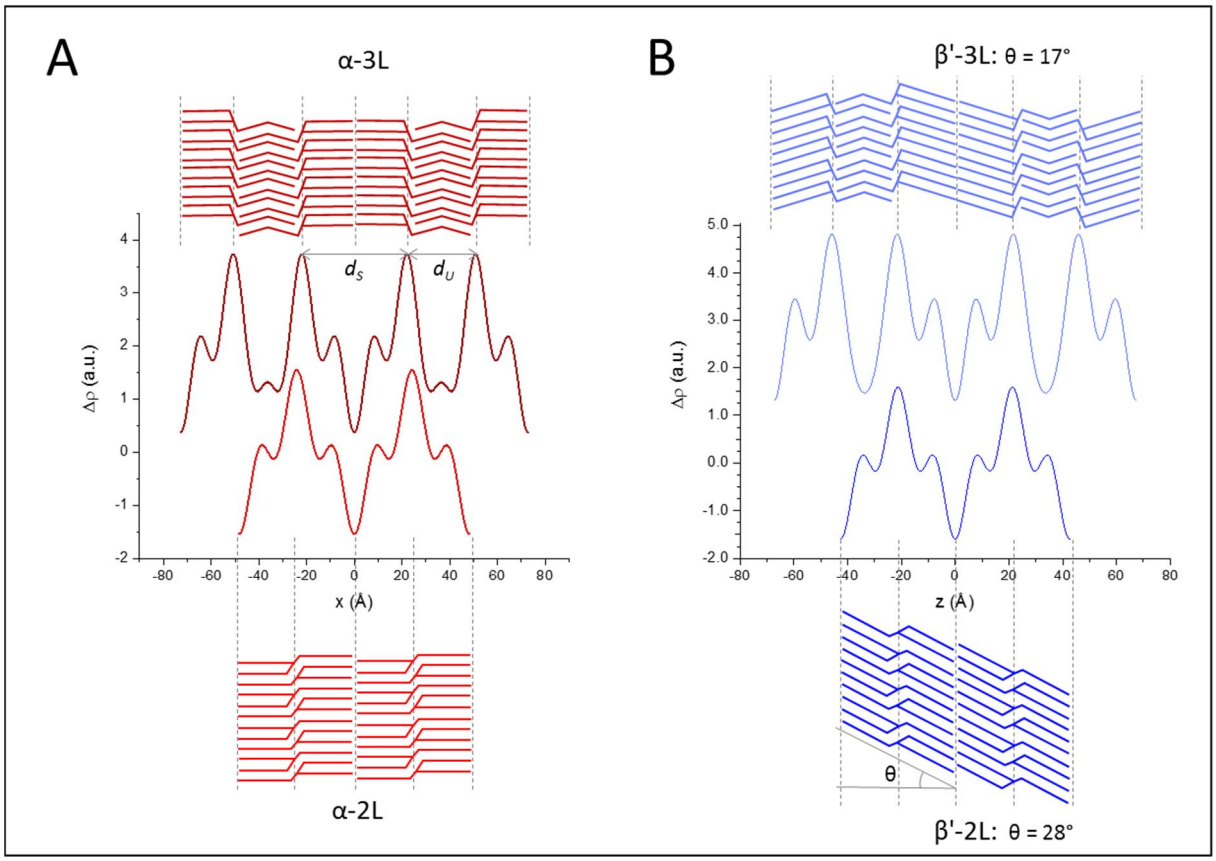

Figure 5. Electron density profiles (EDPs) of buffalo milk fat at -10 °C. (A) The α-2L and α-3L polymorphs with *d*-spacings of 48.4 and 72.8 Å (d_S = 44.3 Å), respectively. (B) The β'-2L and β'-3L polymorphs with *d*-spacings of 42.6 and 67.4 Å (d_S = 42.3 Å), respectively. Further details on the determination of the EDPs are given in the Supporting Information in Figure S2 and S3 as well as in Table S2.

Following the chain length concept for the α-2L form, N_C can also be estimated from d_S following Equation 2, but the tilt angle of chains needs to be considered beforehand. For the unsaturated-rich chain region, d_U, we can also formulate a rough estimate for N_C:

$$N_C \geq (d_U - 8\text{Å})/1.27\ \text{Å}, \qquad \text{(Eq. 3)}$$

where again, 1.27 Å refers to projected the C-C bond length and the glycerol backbone extension is considered to be 8 Å. However, due to expected fatty acid with cis double bonds

in this region, which give rise to kinked acyl chains, the Eq. 3 only gives a lower bound estimate for N_C.

Confirming the DSC thermograms, the α-2L phase consistently nucleates before the α-3L crystalline form in cooling (cp. Figure 3 and 6). Therefore, we suppose that both crystals are formed from two different TAG fractions, with the α-2L containing TAG with relatively higher melting points. Using Eq. 1, the α-2L (48.4 Å) structure has been estimated to contain about 15.9 carbon atoms in average. This is slightly lower than what was found by Lopez et al.[11], who estimated for the similar α-2L species 16.7 carbon atoms on average. As the α-2L polymorph is nucleating at relatively higher temperature, it is reasonable to predict that this structure is constituted mostly of saturated fatty acids which have higher melting point than its unsaturated counterpart. In fact, the average number of 16 carbon atoms corresponds perfectly to palmitic (C16:0) fatty acids or to combinations of for instance myristic (C14:0) and stearic (18:0). TAGs such as MPP, PPP, SPS, and PPS might therefore part of in this α-2L structure.

Using a similar approach as for the α-2L polymorph, the saturated bilayer region of BMF α-3L (d_S =44.3 Å; Figure 5A) was found to have an average lipid length of 14.3 carbon atoms. We assumed again a zero-chain tilt angle also for this α-phase. Considering the diverse population of TAGs in milk fat, we estimated that the saturated region in the 3L structure is likely to comprise of a wider range of saturated fatty acids, such as lauric (12:0), myristic (14:0) and palmitic (16:0). In contrast, the estimated d_U thickness was 28.5 Å, which corresponds to chains with $N_C \geq 16$ carbon atoms as calculated by Eq. 3. Because this region of the lamella contains mainly unsaturated fatty acids, the number of carbon atoms estimated can only be associated with sufficiently long unsaturated chains present in milk fat such as oleic (18:1) and linoleic (18:2) acids. Thus, we expect that the α-3L structure is formed by several TAGs consisting of both saturated and unsaturated fatty acids such as PML, PMO, POO, OMO, PLO, etc. This can also explain the lower nucleation temperature. Further evidence is indicated by the bigger peak-fraction area in the crystallisation thermogram of α-3L compared to α-2L (Figure 3 A, B, C), which shows a higher portion of TAGs involved in the second crystallisation event.

It is worth pointing out, that the electron density profile (EDP) of the α-3L phase in BMF is different from other published α-3L phases, such as for SOS.[45] While the 3L-α polymorph of BMF clearly displays a perfect hexagonal chain packing as known for all α polymorphs, the long spacings and corresponding amplitudes, F_h, are strikingly similar to the 3L-γ polymorph of SOS[45] (see Table S3 in the SI). In contrast, the electron density profile of the 3L-α polymorph

of SOS is clearly different to the 3L-α polymorph of BMF. In summary, the 3L-α polymorph of BMF displays common α-phase packing of chains combined with commonly known γ-phase stacking of TAGs.

Figure 4 also displays a polymorphic transformation from the metastable α-polymorph into the more stable β'-polymorph. This is confirmed by the disappearance of the α-$3L_1$ peak at q = 0.083 $Å^{-1}$ (75 Å), as well as the vanishing of the overlapping α-$2L_2$ and α-$3L_3$ peaks at q = 0.258 $Å^{-1}$ (24 Å) (we note, however, that this concerns mainly the α-$3L_3$ intensity, because the α-$2L_2$ reflection is very weak in intensity[44]). Furthermore, in the wide angle regime, the appearance of the β'-polymorph was clearly indicated by the presence of an additional, β'-phase characteristic peak at q = 1.649 $Å^{-1}$ (3.81 Å). These polymorphic transitions are further supported by determined fraction curves of the β'-2L and β'-3L phases formations (Figure S4). While both β'-phases start to appear simultaneously, only the α-3L → β'-3L turnover is completed within the experimental window of 5 hours, whereas the α-2L → β'-2L transformation remains incomplete, with reference to our preferred interpretation of having distinct TAG compositions in the 2L and 3L polymorphs, respectively. Nonetheless, the 3L transitional route being completed, whereas the 2L form show only an incomplete turnover is readily understood. 3L phases are energetically favoured in condensing their chain packing during the α- to β-phase transition, because they are less prone to packing frustration. Note, saturated and unsaturated lipids are neatly phase-separated in the 3L-stacking geometry and hence increasing the packing density in the d_S-regime is easier to achieve than in the 2L-phases, where the unsaturated and saturated lipids are irrevocably coexisting in the bilayer region.

The polymorphic transformation from the α to the β' form took place at different times for BMF and CMF. During the isothermal hold at -10 °C, the β'-polymorph in CMF appeared at t = 1 hour, whereas BMF took a further half an hour to develop the β'-polymorph. This indicates slower α to β' polymorph transformation kinetics in BMF, when compared to CMF.

Importantly, we observe the formation of both, the β'-phase with 2L and 3L stacking architecture. However, their lattice spacings are considerable smaller, due to their denser fatty acid chain packing, which is always accompanied by a chain tilt in order to match the molecular areas at the polar/apolar interface. Hence, the 3L-form has a d-spacing of 67 Å and a 2L-form of 39 Å, which compares to d-spacings of 72.8 Å and 48.4 Å of the α-polymorphs. Note, we observed the same β'-2L crystal species with d-spacing of 41 and 43 Å in our thermokinetic experiments (shown in Figure 6 and Figure 7). Lopez et al.[11] reported a similar finding, where

the 2L form (d = 41 Å) has been associated with a β'-polymorph, whilst the 3L form was tentatively identified as the α or β'-polymorph. In the current study, the appearance of the long-spacing peaks in the small angle regime coincided with the appearance of the β'-polymorph peaks in wide angle. Therefore, we concluded that both the 2L (39 Å) and 3L (67 Å) forms are associated with the β'-polymorph.

As mentioned above, the 2L- and 3L-form of the α polymorphs (hexagonal packing) are most likely characterized by different TAG compositions, since the former has a higher melting point. Thus, interpreting the polymorphic transformation from α to β'-polymorph to occur within the same stacking configurations, i.e., α-2L (48.4 Å) → β'-2L (39 Å) and α-3L (72.8 Å) → β'-3L (67 Å) remains to make good sense. This finding was also confirmed in a melting experiment (Figure 7), which shows that the β'-3L has lower melting temperature than the β'-2L.

The shorter d-spacing of the β'-polymorph indicates a more dense packing in this form compared to the α-polymorph. Assuming that both α-crystals do not have a chain tilt, the tilt angles for the β'-2L and β'-3L were estimated to be 28° and 17°, respectively. Corresponding schemes of the EDPs of β'-2L and β'-3L are presented in Figure 5B.

3.4 Nucleation Kinetic

The nucleation kinetics of BMF and CMF were evaluated using three different cooling rates, i.e., 4, 2, and 0.5 °C/min, respectively. The milk fats were fully melted at 60 °C before being subjected to a cooling ramp down to -10 °C. The temperature resolved X-ray diffraction patterns are shown in Figure 6.

When applying a cooling rate of 4 °C/min (Figure 6A and D), both BMF and CMF developed a crystalline structure with a peak at q = 0.131 $Å^{-1}$ (48 Å), at temperatures of 12 and 8 °C, respectively. These structures match the 2L form α-polymorph with hexagonally packed hydrocarbon chains, as indicated by a single strong peak in wide angle at q = 1.510 $Å^{-1}$ (4.16 Å). Subsequently, four distinct peaks were observed in the small angle regime; the strongest one at q = 0.170 $Å^{-1}$ (37 Å). These peaks were identified to belong to the α-3L form with d-spacing of 72.8 Å. This structure was observed at 4 and 0 °C for BMF and CMF, respectively.

With a cooling rate of 2 °C/min (Figure 6B and E), similar trends to the faster cooling were observed. The α-2L crystalline species (48 Å) was nucleated first, at temperatures of 14 and 12

°C for BMF and CMF, respectively. A second crystal lattice associated with the hexagonal packing α-polymorph and 3L stacking form (α-3L) nucleated subsequently, evidenced by the appearance of its 4 orders of diffraction peaks in the small angle regime. The BMF α-3L nucleated at a temperature of 8 °C, while CMF nucleated at 6 °C.

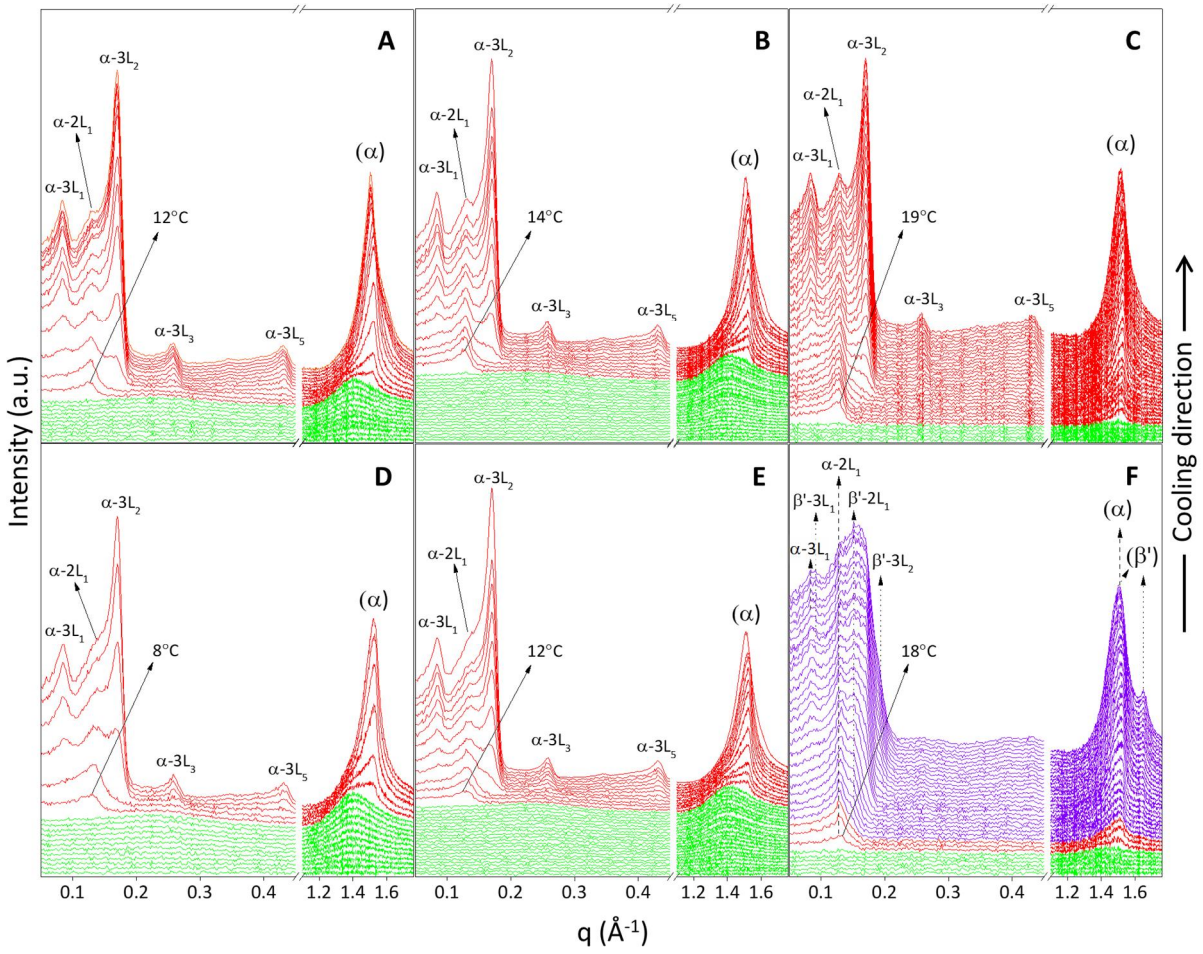

Figure 6. Temperature-resolved X-ray diffraction patterns recorded at small and wide angles on cooling from 60 °C to -10 °C. (A) buffalo milk fat (BMF) on cooling 4 °C/min (B) BMF on cooling 2 °C/min (C) BMF on cooling -0.5 °C/min (D) cow milk fat (CMF) on cooling 4 °C/min (E) CMF on cooling 2 °C/min (F) CMF on cooling 0.5 °C/min. (C) and (F) are presented only from 25 °C to -10 °C for clarity. Green lines: liquid phase, red lines: α-polymorph, purple lines: α- and β'- polymorph.

The results from crystallization experiments at 4 and 2 °C/min cooling rate showed that the α-2L consistently nucleated before the α-3L crystalline form. This is due to the aforementioned evidences that the α-2L most likely comprises long chain saturated TAGs, such as SPS and PPS; the α-3L crystal is instead made of a combination of medium to long saturated FAs and unsaturated FAs (oleic or linoleic acids). SPS and PPS are the TAGs with highest melting points among all TAG species in milk fat, thus providing the highest thermodynamic driving force for

nucleation during the cooling profiles. For this same reason, we were expecting that the BMF α-2L would nucleate at higher temperature, when compared to CMF.

The X-ray scattering data are in agreement with the thermal analysis results, which showed higher nucleation temperatures in BMF than CMF for both exothermic peaks associated with the α-2L and α-3L crystal lattices (Figure 3, Table 3). However, the crystallisation events were not observed at the exact same temperatures. For instance, at 2 °C/min cooling rate, the nucleation temperatures for the α-2L were 18.7 and 16.6 °C for BMF and CMF, respectively. Whereas, the nucleation temperatures recorded in the X-ray scattering experiment for the same cooling rate were 14 and 12 °C for BMF and CMF, respectively. It should be noted that the amount of sample and the geometry of the sample holder of the DSC and X-ray equipment were different, which could be the reason for this discrepancy.

Different behaviours of BMF and CMF were observed using a cooling rate of 0.5 °C/min (Figure 6C and F). In BMF, two crystal lattices associated with the α-2L (48.5 Å) and α-3L (72.8 Å) structures nucleated at temperatures of 19 and 12 °C. The same trend is observed in our thermal analysis, where lower cooling rates resulted in higher nucleation temperatures. Despite the difference in nucleation temperatures, with all applied methods we observed a consistent crystallisation behaviour at all three cooling rates for BMF.

On the other hand, CMF behaved differently from BMF at the lowest cooling rate of 0.5 °C/min. In fact, this sample developed at least four different crystal lattices. The α-2L (48 Å) crystalline nucleated at a temperature of 18 °C. Subsequently, starting from around 15 °C, three additional crystal structures were observed. The exact nucleation temperatures of these other crystal structures were hard to pinpoint due to various superimposed diffraction peaks during the phase formations. However, we could identify each nucleated form. The first one was a 3L crystalline structure associated with the hexagonal packing α-polymorph, as indicated by peak at $q = 0.087$ $Å^{-1}$ (d-spacing of 72 Å). Another 3L crystal form with d-spacing of 67 Å could be identified (note, here we used the intense second order peak at $q = 0.190$ $Å^{-1}$ for determining the lattice spacing). This specific crystal lattice was found in neither of the other cooling rates for CMF, nor for any cooling rate used for BMF. We associate this structure with the orthorhombic packing of a β'-polymorph, as evidenced by the presence of the 3.8 Å peak in wide angle. The last identified crystal lattice, observable at $q = 0.153$ $Å^{-1}$ (41 Å), also corresponds to a β'-polymorph with 2L lamellar stacking.

The formation of a β'-polymorph in CMF has been reported in previous studies using anhydrous CMF, where different polymorphic crystalline forms were observed as the function of different cooling rates. Our study is in agreement with Grotenhuis et al.,[10] who found that α-crystallization was favoured for cooling rates ≥ 1.67 °C/min with no β′-polymorph observed. Whereas, the β′-crystallization was observed for cooling rates ≤ 1°C/min. Another study by Lopez et al.[16] did not find a β'-polymorph up to cooling rates of 1°C/min, whilst observed the β′-crystallization at a cooling rate of 0.1 °C/min. It is worth noticing that both Grotenhuis et al.[10] and Lopez et al.[16] used different sample holder and sample volumes compared to the current study. Both factors can affect the kinetics of nucleation and crystal growth; therefore, while a similar behaviour among this study and previous ones can be observed, the actual cooling rates at which different polymorphs can appear might be different.

It is worth noting that BMF has similar TAG species to CMF but still failed to produce the β' form when a slow cooling rate of 0.5 °C/min was applied. A crystallisation study involving olein- and stearin-rich fractions of anhydrous CMF[11] showed that when these fractions were subjected to a cooling rate of 1°C/min, the olein-rich fraction favoured the crystallisation of the pure α-form, whilst the stearin-rich sample produced both α- and β'-polymorphs. The study indicated that crystallization of the β' crystal structure is more likely to occur in the presence of saturated or higher-melting TAGs, such as given in the stearin-rich fraction. Therefore, the failure in producing the β'-polymorph, is somewhat contradicting the fact that BMF contains a higher amount of saturated TAGs compared to CMF. One possible explanation is that BMF has a higher olein fraction as well, when compared to CMF; thus offsetting the effect of a higher saturated TAG content. We estimated the amount of olein and stearin in CMF and BMF by looking at the TAG composition. Our results in Figure 2 show that BMF has a higher content of high-molecular weight TAGs (associated to stearin) and low-molecular weight TAGs (associated to olein) compared to CMF. The total weight fraction for the high-molecular weight TAG was 18.1%, whilst for the low-molecular weight TAG it was 48.8%. Therefore, we can estimate a higher olein content in BMF, which could explain the absence of the β'-polymorph for slow cooling rates (Figure 6C) and slower kinetics of α- to β'-transition under isothermal condition (Figure 4). Nevertheless, further studies are needed to confirm this conjecture.

3.5 Kinetics of melting and β-polymorph identification

Figure 7 shows the X-ray diffraction patterns on heating at 2 °C/min of frozen samples of BMF and CMF. An orthorhombic lateral packing of the β'-polymorph was dominant in both milk fats, as shown by the presence of two peaks in the wide angle, i.e., referring to the short spacings of 4.2 and 3.81 Å. Two crystal lattices corresponding to a 2L and a 3L lamellar stacking conformation with *d*-spacing of 42.9 and 64.2 Å were observed. Furthermore, we observed an additional crystal lattice in the small angle regime of BMF, with *d*-spacing of 53 Å. We identified this crystal lattice as a 3L stacking structure. This identification is in agreement with Lopez et al.[16] , where a crystal lattice with *d*-spacing of 54 Å was observed in anhydrous CMF conditioned at 4 °C for 5 days.

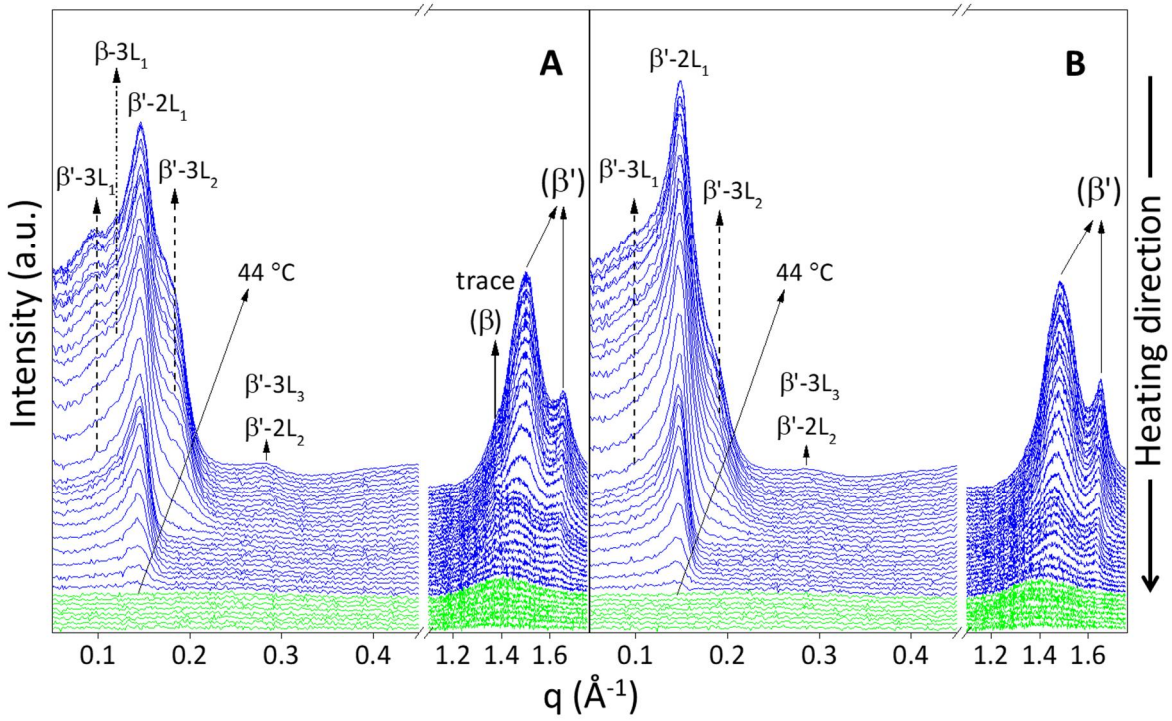

Figure 7. Temperature-resolved X-ray diffraction patterns of (A) buffalo milk fat and (B) cow milk fat heating from -10 to 60°C at 2 °C/min after being frozen for 3 weeks. Green lines: liquid phase, blue lines: β'- polymorph.

Lopez et al.[16] did not associate this 3L structure with any specific polymorph type. However, in the current study, we can infer that it is a triclinic packing corresponding to a β-polymorph. As shown in the wide angle regime (Figure 7A), the appearance of the 3L form in BMF was accompanied by a peak at q = 1.376 Å^{-1} (4.6 Å), which corresponds to the most intense β-polymorph short spacing. Similar spacings, both concerning small and wide angle regimes, were not found in CMF (Figure 7B). At freezer temperature, BMF has more liquid oil portion

due to its higher low melting point TAGs than that of CMF. The presence of liquid oil allows better diffusion of the milk fat TAGs to form more stable β-crystals, as also reported by Wright et al.[49]

The *d*-spacing of the β-3L (53 Å) observed here is very small compared to a well-known β-crystals of SOS which is 64.5 Å[45]. In order to shed some light on this structure, we simulated the EDP of the β-3L (see Figure S5 in the SI). Since the *d*-spacing was the only experimental observable parameter, the simulated EDP based on two rigorous assumptions. Firstly, the saturated bilayer was assumed to comprise 16 carbon atoms saturated fatty acid in average. Note, palmitic acid is the most abundant FA in BMF.[4,28] Secondly, the chain tilt angle for the β-phase was assumed to be 36° as confirmed in literature for SOS.[45] Other SOS-rich samples[50] display chain tilt angles of 33° and 36° for the β'-3L and β-3L polymorph, respectively. Thus, we limited possible chain tilts in the β-3L polymorph in BMF to vary from 33 to 36°, and consequently find d_S to vary in the range of 39-41 Å from which d_U values from 12-14 Å follow. The monolayer unsaturated chain region is very thin, with an average chain length of about 4 carbon atoms (Eq. 3). Milk fat is abundant in short chain fatty acids such as butyric (C4) and caproic (C6) acids. Hence, it is very tempting to come to the conclusion that this β-3L (53 Å) crystal lattice comprises of the TAGs containing short fatty acids being present in the d_U regions, and thus entirely different from those contributing to α-3L and β'-3L polymorphs. This tentative conclusion also aligns well with the fact that BMF has a higher content of butyric-containing TAGs (Figure 2), which might explain the appearance of the β-3L in BMF but not in CMF. The summary of all polymorphs and the associating crystal lattices found in this work is given in Table 5.

Table 5. Summary of all polymorphs of buffalo milk fat and cow milk fat.

Structure	*d*-spacing (Å)	d_S (Å)	d_U (Å)	Contributing TAG
α-2L	48-49	-	-	Long chain saturated TAG (e.g., PPP, PPS and SPS)
α-3L	72-73	44.3	28.5	TAG containing medium-long saturated FAs and long chain mono/poly-unsaturated FAs (e.g., PLaO, PCO, PPO)
β'-2L	39-43	-	-	Proposed compositional similarity to α-2L
β'-3L	64-67	42.3	25.1	Proposed compositional similarity to α-3L
β-3L	53	39-41	12-14	Proposed: TAG containing short chain FAs (e.g., BuPS, BuPP, CoMP)

On heating at 2 °C/min, the peak intensity in the small angle regime decreased and finally reached a constant value, indicating the melt of the crystals (Figure 7). The β'-3L crystal disappeared at around 22 °C and the β'-2L final melting temperature was around 44 °C. There was no observable difference in melting temperatures for each polymorphs of BMF and CMF. Finally, while the β-3L (53 Å) peak was subtle and the intensity too poor to pinpoint its exact melting point, we clearly observed that the wide angle 4.6 Å (β) peak persisted until 44 °C.

3.6 Crystal microstructure

Micrographs of BMF and CMF upon cooling at 2 and 0.5 °C/min are presented in Figure 8. In general, both milk fats showed a higher rate of nucleation, but slower crystal growth at the faster cooling rate. Faster cooling rates induce nucleation at higher levels of undercooling, thus generating a larger number of nuclei. Moreover, as the cooling was continued further to -10°C, the nuclei growth was hindered not only by their dense population but also by the increasing viscosity of the sample, which impairs crystal growth.[51]

At a cooling rate of 2 °C/min (Figure 8A and B), the BMF and CMF samples both show characteristics clusters of needle-like crystals (spherulites) of different average equivalent diameter (around 7 μm for BMF and of 6 μm for CMF). The faster nucleation rate for CMF in this cooling conditions, highlighted by the presence of a larger number of clusters, might be due to the lower content of low melting TAGs compared to BMF, which nucleate slower than the mid- and high-melting TAGs. This behaviour is in accordance with what found by Ramel and Marangoni [52] on ternary mixtures of high-, mid- and low-melting fraction of milk fat.

A slower cooling rate of 0.5 °C/min (Figure 8C and D) showed less clusters of larger size for both, BMF and CMF. The BMF spherulites were around 19.5 μm in diameter, while the CMF had an average diameter of 25.3 μm and displayed a dendritic/snow-flake morphology. These results show a difference in the growth and nucleation rates at slow cooling rates between BMF and CMF; however, the reason for this behaviour is still unclear and requires further investigation.

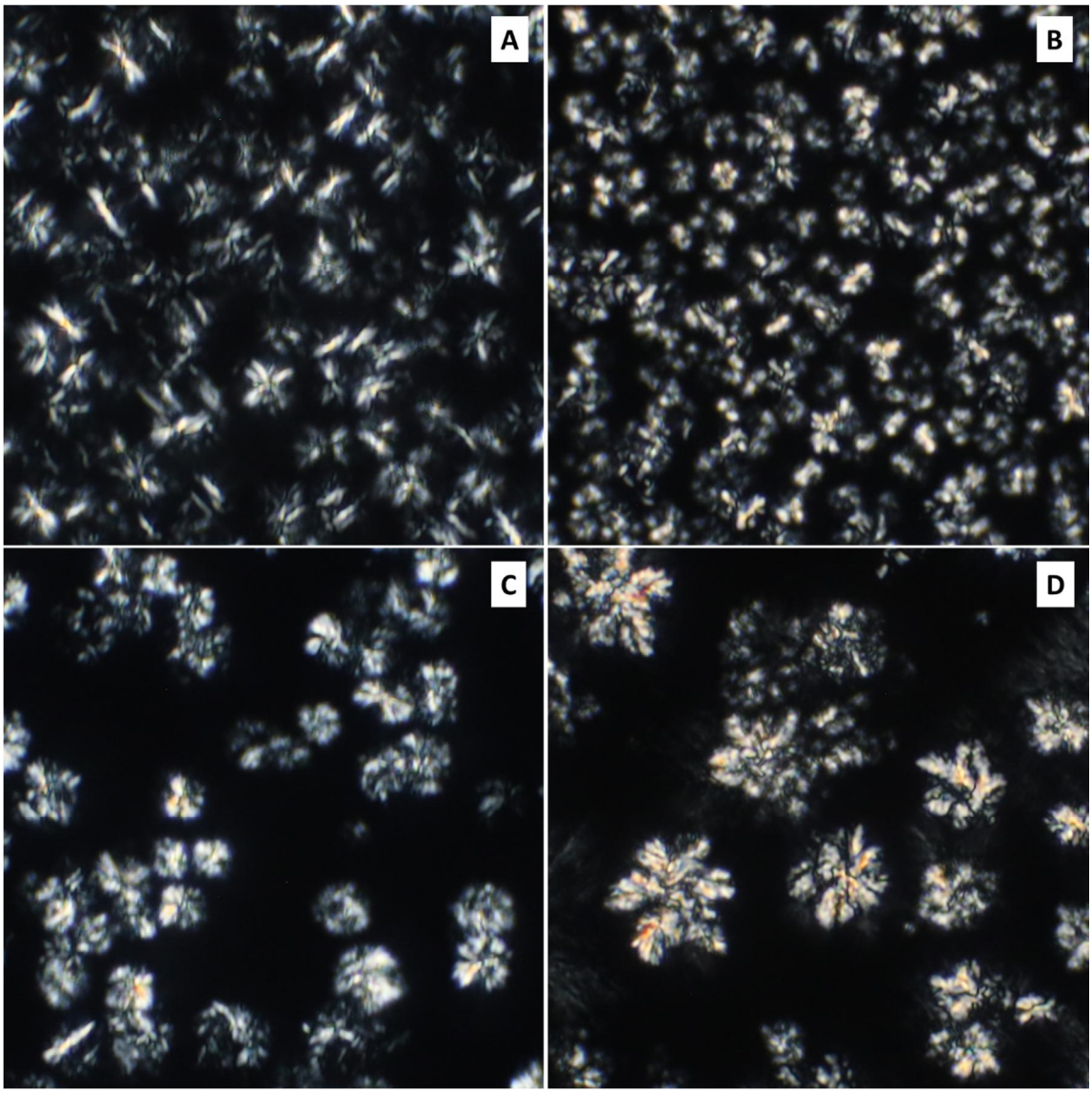

Figure 8. Polarized light micrographs taken at 15°C of (A) buffalo milk fat (BMF), (B) cow milk fat (CMF) on cooling at 2°C/min and (C) BMF, (D) CMF on cooling at 0.5°C/min from melt at 60°C. Dimensions on each image correspond to 200x200 microns.

4 Conclusions

For the first time, the BMF crystallisation has been detailed in great depths, combining mass-spectroscopy and calorimetry data with nano- as well as microstructural studies. In particular, the extensive small- and wide angle X-ray scattering experiments have revealed the unique dynamic and polymorphic behaviour of BMF. While BMF has similar TAG species as CMF, 20 out of 37 identified TAGs differ significantly in their quantities. Although the nucleation temperatures of BMF are higher, the formation of β'-polymorph in BMF takes longer time than in CMF under isothermal conditions (hold at -10 °C). Similarly, BMF nucleates only α-

polymorphs during slow cooling rates, while CMF forms both, α- and β'-polymorph. The delay of the β'-polymorph formation is potentially caused by the higher portion of olein-fraction or low molecular weight TAGs in BMF, while the higher nucleation and melting point temperatures in BMF are a consequence of the bigger portion of saturated TAGs. We further provided evidence for a specific segregation in the milk fat crystallisation process. The polymorphic transformations seem to occur within the same lamellar structures, and hence driven by the same TAG groups, i.e., leading to two parallel transitions: α-2L → β'-2L and α-3L → β'-3L. This is supported by our detailed nanostructural analysis as well as by the higher nucleation and melting temperatures of α-2L and β'-2L, respectively, which match the characteristic TAG groups consisting of mainly saturated species. Furthermore, we proposed a novel interpretation of the three chain length β-polymorph (*d*-spacing 53 Å), which is likely to be formed by asymmetrical TAGs containing butyric acids. In addition to the difference in nanostructure, BMF also displayed different microstructure than CMF (spherulites *vs.* snowflake like crystals). As such, this study provides profound insight into the crystallisation behaviour of different milk fats as influenced by its TAG compositional difference.

Associated Content

Supporting Information: The Supporting Information is available free of charge at XXX.

Additional mass spectroscopy data and further small and wide-angle X-ray scattering data analysis are provided, including 5 figures and 3 tables (PDF).

Acknowledgements

The authors are grateful for the funding provided by Indonesian Endowment Fund for Education (LPDP) in the form of full scholarship for Ph.D. study of Yoga Pratama. Dr Simone acknowledge the Royal Society, grant ref. no. INF\R2\192018, for funding.

References

(1) FAO. *FAOSTAT Statistical Database*; Rome, 2019.

(2) Murtaza, M. A.; Pandya, A. J.; Khan, M. H. M. Buffalo Milk: Buffalo Milk Utilization for Dairy Products. In *Handbook of Milk of Non-Bovine Mammals: Second Edition*; Park, Y. W., Haenlein, G. F. W., Wendorff, W. L., Eds.; Wiley Blackwell: Oxford, UK, 2017; pp 284–342. https://doi.org/10.1002/9781119110316.ch4.2.

(3) Angelis, M. De; Gobbetti, M. Pasta-Filata Cheeses: Traditional Pasta-Filata Cheese. In *Encyclopedia of Dairy Sciences*; Fuquay, J. W., Fox, P. F., McSweeney, P. L. H., Eds.; Academic Press: Oxford, 2011; pp 1:745-752.

(4) Abd El-Salam, M. H.; El-Shibiny, S. A Comprehensive Review on the Composition and Properties of Buffalo Milk. *Dairy Sci. Technol.* **2011**, *91* (6), 663–699. https://doi.org/10.1007/s13594-011-0029-2.

(5) Gantner, V.; Mijić, P.; Baban, M.; Škrtić, Z.; Turalija, A. The Overall and Fat Composition of Milk of Various Species. *Mljekarstvo* **2015**, *65* (4), 223–231. https://doi.org/10.15567/mljekarstvo.2015.0401.

(6) Zhou, L.; Tang, Q.; Wasim Iqbal, M.; Xia, Z.; Huang, F.; Li, L.; Liang, M.; Lin, B.; Qin, G.; Zou, C. A Comparison of Milk Protein, Fat, Lactose, Total Solids and Amino Acid Profiles of Three Different Buffalo Breeds in Guangxi, China. *Ital. J. Anim. Sci.* **2018**, *17* (4), 873–878. https://doi.org/10.1080/1828051X.2018.1443288.

(7) Martini, S.; Marangoni, A. G. Microstructure of Dairy Fat Products. In *Structure of Dairy Products*; Tamime, A., Ed.; Blackwell Publishing Ltd: Oxford, 2007; pp 72–103.

(8) Idziak, S. H. J. Powder X-Ray Diffraction of Triglycerides in the Study of Polymorphism. In *Structure-Function Analysis of Edible Fats*; Elsevier, 2018; pp 73–99. https://doi.org/10.1016/B978-0-12-814041-3.00003-4.

(9) D'Souza, V.; DeMan, J. M.; DeMan, L. Short Spacings and Polymorphic Forms of Natural and Commercial Solid Fats: A Review. *J. Am. Oil Chem. Soc.* **1990**, *67* (11), 835–843. https://doi.org/10.1007/BF02540502.

(10) Grotenhuis, E. Ten; Van Aken, G. A.; Van Malssen, K. F.; Schenk, H. Polymorphism of Milk Fat Studied by Differential Scanning Calorimetry and Real-Time X-Ray Powder Diffraction. *JAOCS, J. Am. Oil Chem. Soc.* **1999**, *76* (9), 1031–1039.

https://doi.org/10.1007/s11746-999-0201-5.

(11) Lopez, C.; Bourgaux, C.; Lesieur, P.; Riaublanc, A.; Ollivon, M. Milk Fat and Primary Fractions Obtained by Dry Fractionation. 1. Chemical Composition and Crystallisation Properties. *Chem. Phys. Lipids* **2006**. https://doi.org/10.1016/j.chemphyslip.2006.06.002.

(12) Tzompa-Sosa, D. A.; Ramel, P. R.; Van Valenberg, H. J. F.; Van Aken, G. A. Formation of β Polymorphs in Milk Fats with Large Differences in Triacylglycerol Profiles. *J. Agric. Food Chem.* **2016**, *64* (20), 4152–4157. https://doi.org/10.1021/acs.jafc.5b05737.

(13) Shi, Y.; Smith, C. M.; Hartel, R. W. Compositional Effects on Milk Fat Crystallization. *J. Dairy Sci.* **2001**, *84* (11), 2392–2401. https://doi.org/10.3168/jds.S0022-0302(01)74688-7.

(14) Van Aken, C. A.; Ten Grotenhuis, E.; Van Langevelde, A. J.; Schenk, H. Composition and Crystallization of Milk Fat Fractions. *JAOCS, J. Am. Oil Chem. Soc.* **1999**, *76* (11), 1323–1331. https://doi.org/10.1007/s11746-999-0146-8.

(15) Marangoni, A. G.; Lencki, R. W. Ternary Phase Behavior of Milk Fat Fractions. *J. Agric. Food Chem.* **1998**, *46* (10), 3879–3884. https://doi.org/10.1021/jf9801668.

(16) Lopez, C.; Lesieur, P.; Bourgaux, C.; Ollivon, M. Thermal and Structural Behavior of Anhydrous Milk Fat. 3. Influence of Cooling Rate. *J. Dairy Sci.* **2005**, *88* (2), 511–526. https://doi.org/10.3168/jds.S0022-0302(05)72713-2.

(17) Campos, R.; Narine, S. S.; Marangoni, A. G. Effect of Cooling Rate on the Structure and Mechanical Properties of Milk Fat and Lard. *Food Res. Int.* **2002**, *35* (10), 971–981. https://doi.org/10.1016/S0963-9969(02)00159-X.

(18) Mazzanti, G.; Marangoni, A. G.; Idziak, S. H. J. Synchrotron Study on Crystallization Kinetics of Milk Fat under Shear Flow. *Food Res. Int.* **2009**, *42* (5–6), 682–694. https://doi.org/10.1016/j.foodres.2009.02.009.

(19) Wright, A. J.; Hartel, R. W.; Narine, S. S.; Marangoni, A. G. Effect of Minor Components on Milk Fat Crystallization. *JAOCS, J. Am. Oil Chem. Soc.* **2000**, *77* (5), 463–475. https://doi.org/10.1007/s11746-000-0075-8.

(20) Wright, A. J.; McGauley, S. E.; Narine, S. S.; Willis, W. M.; Lencki, R. W.; Marangoni, A. G. Solvent Effects on the Crystallization Behavior of Milk Fat Fractions. *J. Agric. Food Chem.* **2000**, *48* (4), 1033–1040. https://doi.org/10.1021/jf9908244.

(21) Van Aken, G. A.; Visser, K. A. Firmness and Crystallization of Milk Fat in Relation to Processing Conditions. *J. Dairy Sci.* **2000**, *83* (9), 1919–1932. https://doi.org/10.3168/jds.S0022-0302(00)75067-3.

(22) Lopez, C. Crystallization Properties of Milk Fats. In *Crystallization of Lipids: Fundamentals and Applications in Food, Cosmetics and Pharmaceuticals*; John Wiley & Sons, Ltd: Chichester, UK, 2018; pp 283–321. https://doi.org/10.1002/9781118593882.ch10.

(23) Ramel, P. R.; Marangoni, A. G. Insights into the Mechanism of the Formation of the Most Stable Crystal Polymorph of Milk Fat in Model Protein Matrices. *J. Dairy Sci.* **2017**, *100* (9), 6930–6937. https://doi.org/10.3168/jds.2017-12758.

(24) Mazzanti, G.; Guthrie, S. E.; Sirota, E. B.; Marangoni, A. G.; Idziak, S. H. J. Effect of Minor Components and Temperature Profiles on Polymorphism in Milk Fat. *Cryst. Growth Des.* **2004**, *4* (6), 1303–1309. https://doi.org/10.1021/cg0497602.

(25) Sato, K. Molecular Aspects in Fat Polymorphism. In *Crystallization and Solidification Properties of Lipids*; Widlak, N., Hartel, R., Narine, S., Eds.; AOCS Press: Champaign, Illinois, Illinois, 2001; pp 1–17.

(26) Tzompa-Sosa, D. A.; Meurs, P. P.; van Valenberg, H. J. F. Triacylglycerol Profile of Summer and Winter Bovine Milk Fat and the Feasibility of Triacylglycerol Fragmentation. *Eur. J. Lipid Sci. Technol.* **2018**, *120* (3), 1700291. https://doi.org/10.1002/ejlt.201700291.

(27) Larsen, M. K.; Andersen, K. K.; Kaufmann, N.; Wiking, L. Seasonal Variation in the Composition and Melting Behavior of Milk Fat. *J. Dairy Sci.* **2014**, *97* (8), 4703–4712. https://doi.org/10.3168/jds.2013-7858.

(28) Ménard, O.; Ahmad, S.; Rousseau, F.; Briard-Bion, V.; Gaucheron, F.; Lopez, C. Buffalo vs. Cow Milk Fat Globules: Size Distribution, Zeta-Potential, Compositions in Total Fatty Acids and in Polar Lipids from the Milk Fat Globule Membrane. *Food*

Chem. **2010**, *120* (2), 544–551. https://doi.org/10.1016/J.FOODCHEM.2009.10.053.

(29) Amara-Dali, W. Ben; Karray, N.; Lesieur, P.; Ollivon, M. Anhydrous Goat's Milk Fat: Thermal and Structural Behavior. 1. Crystalline Forms Obtained by Slow Cooling. *J. Agric. Food Chem.* **2005**, *53* (26), 10018–10025. https://doi.org/10.1021/jf051529o.

(30) Amara-Dali, W. Ben; Lesieur, P.; Artzner, F.; Karray, N.; Attia, H.; Ollivon, M. Anhydrous Goat's Milk Fat: Thermal and Structural Behaviors Studied by Coupled Differential Scanning Calorimetry and X-Ray Diffraction. 2. Influence of Cooling Rate. *J. Agric. Food Chem.* **2007**, *55* (12), 4741–4751. https://doi.org/10.1021/jf063210p.

(31) Karray, N.; Lopez, C.; Lesieur, P.; Ollivon, M. Dromedary Milk Fat: Thermal and Structural Properties 1. Crystalline Forms Obtained by Slow Cooling. *Lait* **2004**, *84* (4), 399–416. https://doi.org/10.1051/lait:2004014.

(32) Karray, N.; Lopez, C.; Lesieur, P.; Ollivon, M. Dromedary Milk Fat: Thermal and Structural Properties 2. Influence of Cooling Rate. *Lait* **2005**, *85* (6), 433–451. https://doi.org/10.1051/lait:2005034.

(33) Mottram, H. R.; Evershed, R. P. Elucidation of the Composition of Bovine Milk Fat Triacylglycerols Using High-Performance Liquid Chromatography-Atmospheric Pressure Chemical Ionisation Mass Spectrometry. *J. Chromatogr. A* **2001**, *926* (2), 239–253. https://doi.org/10.1016/S0021-9673(01)01048-2.

(34) Gastaldi, D.; Medana, C.; Giancotti, V.; Aigotti, R.; Dal Bello, F.; Baiocchi, C. HPLC-APCI Analysis of Triacylglycerols in Milk Fat from Different Sources. *Eur. J. Lipid Sci. Technol.* **2011**, *113* (2), 197–207. https://doi.org/10.1002/ejlt.201000068.

(35) Zhou, Q.; Gao, B.; Zhang, X.; Xu, Y.; Shi, H.; Yu, L. Chemical Profiling of Triacylglycerols and Diacylglycerols in Cow Milk Fat by Ultra-Performance Convergence Chromatography Combined with a Quadrupole Time-of-Flight Mass Spectrometry. *Food Chem.* **2014**, *143*, 199–204. https://doi.org/10.1016/j.foodchem.2013.07.114.

(36) Ten-Doménech, I.; Beltrán-Iturat, E.; Herrero-Martínez, J. M.; Sancho-Llopis, J. V.; Simó-Alfonso, E. F. Triacylglycerol Analysis in Human Milk and Other Mammalian Species: Small-Scale Sample Preparation, Characterization, and Statistical

Classification Using HPLC-ELSD Profiles. *J. Agric. Food Chem.* **2015**, *63* (24), 5761–5770. https://doi.org/10.1021/acs.jafc.5b01158.

(37) Arumughan, C.; Narayanan, K. M. Triacylglycerol Composition of Buffalo Milk Fat. *J. Dairy Res.* **1982**, *49* (1), 81–85. https://doi.org/10.1017/S0022029900022159.

(38) Smiddy, M. A.; Huppertz, T.; van Ruth, S. M. Triacylglycerol and Melting Profiles of Milk Fat from Several Species. *Int. Dairy J.* **2012**, *24* (2), 64–69. https://doi.org/10.1016/j.idairyj.2011.07.001.

(39) Penchev, P.; Ilieva, Y.; Ivanova, T.; Kalev, R. Fatty Acid Composition of Buffalo and Bovine Milk as Affected by Roughage Source - Silage versus Hay. *Emirates J. Food Agric.* **2016**, *28* (4), 1. https://doi.org/10.9755/ejfa.2015-11-974.

(40) Ganguli, N. C.; Jain, M. K. Ghee: Its Chemistry, Processing and Technology. *J. Dairy Sci.* **1973**, *56* (1), 19–25. https://doi.org/10.3168/jds.S0022-0302(73)85109-4.

(41) Zeb, A.; Murkovic, M. Analysis of Triacylglycerols in Refined Edible Oils by Isocratic HPLC-ESI-MS. *Eur. J. Lipid Sci. Technol.* **2010**, *112*, 844–851. https://doi.org/10.1002/ejlt.201000064.

(42) Norman Dyson. *Chromatographic Integration Methods*, second.; Smith, R. M., Ed.; The Royal Society of Chemistry: Cambridge, 1998.

(43) Li, N. Y. D.; Perutková, Š.; Iglič, A.; Rappolt, M. My First Electron Density Map: A Beginner's Guide to Small Angle X-Ray Diffraction. *Elektroteh. Vestnik/Electrotechnical Rev.* **2017**, *84* (3), 69–75.

(44) Ladd Parada, M.; Sadeghpour, A.; Vieira, J.; Povey, M.; Rappolt, M. Global Small-Angle X-Ray Scattering Data Analysis of Triacylglycerols in the α-Phase (Part II). *J. Phys. Chem. B* **2018**, *122* (45), 10330–10336. https://doi.org/10.1021/acs.jpcb.8b06708.

(45) Mykhaylyk, O. O.; Hamley, I. W. The Packing of Triacylglycerols from SAXS Measurements: Application to the Structure of 1,3-Distearoyl-2-Oleoyl-Sn-Glycerol Crystal Phases. *J. Phys. Chem. B* **2004**, *108* (23), 8069–8083. https://doi.org/10.1021/jp0379704.

(46) Deffense, E. Milk Fat Fractionation Today: A Review. *J. Am. Oil Chem. Soc.* **1993**, *70*

(12), 1193–1201. https://doi.org/10.1007/BF02564225.

(47) Lopez, C.; Bourgaux, C.; Lesieur, P.; Ollivon, M. Coupling of Time-Resolved Synchrotron X-Ray Diffraction and DSC to Elucidate the Crystallisation Properties and Polymorphism of Triglycerides in Milk Fat Globules. *Lait* **2007**, *87* (4–5), 459–480. https://doi.org/10.1051/lait:2007018.

(48) Nagle, J. F.; Tristram-Nagle, S. Structure of Lipid Bilayers. *Biochim. Biophys. Acta - Rev. Biomembr.* **2000**, *1469* (3), 159–195. https://doi.org/10.1016/S0304-4157(00)00016-2.

(49) Wright, A. J.; Batte, H. D.; Marangoni, A. G. Effects of Canola Oil Dilution on Anhydrous Milk Fat Crystallization and Fractionation Behavior. *J. Dairy Sci.* **2005**, *88* (6), 1955–1965. https://doi.org/10.3168/jds.S0022-0302(05)72871-X.

(50) Gregersen, S. B.; Povey, M. J. W.; Andersen, M. D.; Hammershøj, M.; Rappolt, M.; Sadeghpour, A.; Wiking, L. Acoustic Properties of Crystallized Fat: Relation between Polymorphic Form, Microstructure, Fracturing Behavior, and Sound Intensity. *Eur. J. Lipid Sci. Technol.* **2016**, *118* (9), 1257–1270. https://doi.org/10.1002/ejlt.201500435.

(51) Himawan, C.; Starov, V. M.; Stapley, A. G. F. Thermodynamic and Kinetic Aspects of Fat Crystallization. *Advances in Colloid and Interface Science*. Elsevier September 25, 2006, pp 3–33. https://doi.org/10.1016/j.cis.2006.06.016.

(52) Ramel, P. R.; Marangoni, A. G. Engineering the Microstructure of Milk Fat by Blending Binary and Ternary Mixtures of Its Fractions. *RSC Adv.* **2016**, *6* (47), 41189–41194. https://doi.org/10.1039/c6ra07114g.

For Table of Contents Use Only

The Unique Crystallisation Behaviour of Buffalo Milk Fat

Yoga Pratama, Elena Simone and Michael Rappolt

TOC graphic

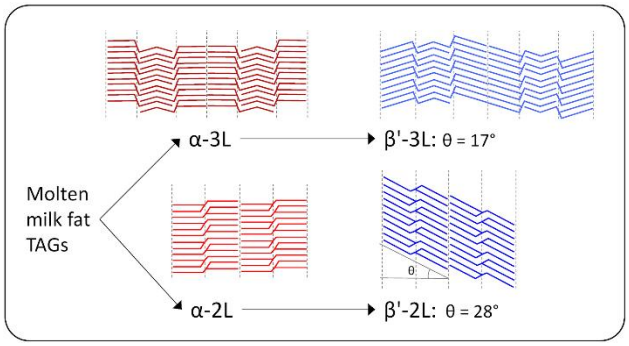

Synopsis

Buffalo milk fat (BMF) contains similar triacylglycerols as cow milk fat (CMF), but in significantly different proportions. BMF has higher nucleation temperature than CMF due to its higher saturated triacylglycerols content; whilst its higher olein proportion is responsible for the delay of the β'-polymorph formation. This unique behaviour is of importance in designing a suitable processing for buffalo milk products.